atmosphere

MDPI

Article

The Diagnostic Analysis of the Thermodynamic Characteristics of Typhoon "Maysak" during Its Transformation Process

Guanbo Zhou [1,*] and Han Du [2]

[1] National Meteorological Center, China Meteorological Administration, Beijing 100081, China
[2] Institute of Atmospheric Physics, Chinese Academy of Sciences, Beijing 100029, China; duhan23@mails.ucas.ac.cn
* Correspondence: zhougb@cma.gov.cn

Abstract: This study utilized high-resolution numerical simulation data from the WRF model to conduct a thermodynamic diagnosis of the process by which Typhoon "Maysak" transformed and merged with the Northeast Cold Vortex. The results indicated that the continuous intrusion of cold vortex air and the relative cold advection formed by the typhoon's movement led to the demise of the typhoon's warm core structure. The low-level low-pressure convergence and upper-level high-pressure divergence structure disappeared. After the transformation and merging with the Northeast Cold Vortex, the cyclone became cold throughout the entire layer, with a cold center appearing at low levels. During the process of the typhoon's transformation and merging with the Northeast Cold Vortex, cold air accumulated near the low levels of the cyclone, causing the pseudo-adiabatic potential temperature lines to tilt and resulting in the slanted development of vertical vorticity in the mid-levels of the cyclone. After the typhoon transformed and merged with the Northeast Cold Vortex, the positive vertical vorticity advection at the bottom of the upper-level cold vortex trough promoted the cyclone's development directly from the mid-levels to the upper levels, while the jet stream at the bottom of the cold vortex trough facilitated the maintenance of the positive vertical vorticity advection. Concurrently, the thermodynamic shear vorticity parameter could describe the typical vertical structure characteristics of the dynamic and thermodynamic fields above the rain area during the typhoon transformation process. In terms of temporal evolution trends, there was a certain correspondence with the development and movement of the ground rain area, and the perturbation thermodynamic divergence parameter had a good indicative effect on the area of heavy rainfall.

Keywords: typhoon; northeast cold vortex; extratropical transition; vertical vorticity; thermodynamic shear vorticity parameter

Citation: Zhou, G.; Du, H. The Diagnostic Analysis of the Thermodynamic Characteristics of Typhoon "Maysak" during Its Transformation Process. *Atmosphere* **2024**, *15*, 1058. https://doi.org/10.3390/atmos15091058

Academic Editors: Mrinal K. Biswas, Jun A. Zhang and Bin Liu

Received: 6 July 2024
Revised: 14 August 2024
Accepted: 18 August 2024
Published: 1 September 2024

1. Introduction

The Northeast Cold Vortex is a large-scale cyclonic circulation system aloft that is uniquely formed under the influence of the specific topography and geographical location of the northeastern region of China. It predominantly occurs in the summer season, characterized by a slow movement, persistence, and a relatively long lifespan, making it one of the main weather systems affecting the northeastern region of China (Zheng Xiuya et al. [1]; Sun Li et al. [2]; Sun Li [3]; Wang Donghai et al. [4]; Hu et al. [5]). The Northeast Cold Vortex often brings cool and rainy weather to the northeastern region during summer and can even lead to flood disasters (Zhang Qingyun et al. [6]; Sun Li et al. [7]; Zhao and Sun [8]; Hu Kaixi et al. [9]). When there is heating in the lower troposphere, the atmosphere under the control of the Northeast Cold Vortex is prone to strong convective instability, which can trigger local severe convective weather, with local hail and heavy rain being more common, and regional heavy rain being less frequent. However, when the Northeast Cold Vortex interacts with systems such as typhoons and cyclones, it can lead to widespread heavy rain or even extreme heavy rain (Zheng Xiuya et al. [1]). For instance, in 2005, the

northeastern region was jointly affected by Typhoon Matsa and the cold vortex system, resulting in significantly above-average summer precipitation in the area (Wang Donghai et al. [4]). Cold eddies provide favorable conditions for heavy rainfall formation, including instability and water vapor transport. The cold vortex has strong oblique pressure and is closely associated with the subtropical low system to the south. The intrusion of dry and cold air strengthens the instability and oblique pressure and may trigger convective activities.

The interaction between the Northeast Cold Vortex and typhoons generally manifests in two forms: the long-distance interaction between the typhoon and the cold vortex, and the northward movement and transformation of the typhoon as it merges with the cold vortex. Ding Yihui et al. [10] pointed out in their study of heavy rain in North China before the 1980s that most of the strong rainstorms in North China often occurred when two or more weather systems interacted with or were superimposed on each other, with the long-distance interaction between the upper-level cold vortex and the typhoon being one of the main forms. Sun Jianhua et al. [11] also showed in their statistical analysis of heavy rain in North China during the summers from 1990 to 1999 that the typhoon and the Northeast Cold Vortex were the main weather systems causing heavy rain in the summer of North China. Cong Chunhua et al. [12], in summarizing the research progress on typhoons' distant heavy rain over the past few decades, pointed out that the long-distance interaction between the typhoons and the Northeast Cold Vortex was one of the main forms of typhoons' distant heavy rain occurrence. The long-distance interaction between typhoons and northeast cold vortex contributes to the generation and maintenance of large-scale summer rainstorm in Northeast China by providing sufficient moisture conditions, creating favorable dynamic uplift and convective instability environment, and promoting the effective convergence of cold and warm air.

The transformation and merging of typhoons into the Northeast Cold Vortex can also lead to extensive heavy rainfall. Yan Minhui et al. [13] analyzed the regional heavy rain process caused by the weakening and transformation of Typhoon "Dandelion" into an extratropical cyclone that merged with the Northeast Cold Vortex in 2004. They found that the heavy rain occurred at the initial stage of the extratropical cyclone, formed after the weakening of Typhoon "Dandelion" from merging with the Northeast Cold Vortex. They pointed out that there were two reasons for the occurrence of this regional strong precipitation: on one hand, the Northeast Cold Vortex changed the direction of the environmental flow field at the periphery of the typhoon, allowing the warm front cloud system on the north side of the weakened extratropical cyclone to move into the northeast region along the steering flow of the upper-level cold vortex. On the other hand, the merging of the typhoon made the originally dry and cold Northeast Cold Vortex rich in water vapor, thereby increasing the level of precipitation. Liang Zhaoming et al. [14] used the local vertical vorticity tendency equation to meticulously analyze the process before and after the transformation of "Dandelion" merging with the Northeast Cold Vortex. They pointed out that after the typhoon transformed and merged with the Northeast Cold Vortex, the positive vertical vorticity advection at the bottom of the upper-level cold vortex trough promoted the cyclone's development directly from the mid-levels to the upper levels, while the jet stream at the bottom of the cold vortex trough facilitated the maintenance of the positive vertical vorticity advection.

As a typical case of combining with the Northeast Cold Vortex and bringing heavy precipitation to the northeast of China in recent years, "Maysak" has been studied by several scholars. Zhou et al. [15] analyzed the mechanism of Typhoon Maysak's land maintenance in comparison with two other northward typhoons, and found that during the influence of Maysak in Northeast China, the blocking high pressure on the east side of the typhoon was maintained stably, and the cold vortex on the west side of the typhoon interacted with it in close proximity and merged with it, and at the same time, the subtropical westerly rapids at high altitude were strengthened, and the configuration of such a circulatory situation was conducive to Typhoon Maysak. This configuration of the circulation situation

field was favorable for the maintenance of the intensity of "Maysak" after its landfall and the impact of wind and rain over a long period of time. In terms of the microphysical mechanism of precipitation, studies have shown that the cold trough has a significant effect on precipitation. Especially in the typhoon eyewall and rainband regions, the analysis of thermodynamic, kinetic, and cloud microphysical characteristics in these regions reveals how the cold trough affects the precipitation intensity. In addition, numerical simulation-based studies have explored the relationship between precipitation intensity and cloud water and snow melting, further understanding the micro-mechanism of precipitation formation (Du et al. [16]). Regarding the metamorphic process of Typhoon Maysak, Ren Li et al. [17] pointed out that its structural evolution characteristics and the cause of heavy rainfall needed to take into account a variety of factors. For example, the changes in the dynamic and thermal structure and water vapor transport characteristics before and after typhoon landfall were crucial for understanding its metamorphic process.

Unlike the indirect effects at a distance (such as remote moisture transport) associated with typhoons and the Northeast Cold Vortex, the process of a typhoon transforming and merging into the Northeast Cold Vortex involves direct interaction (Liang and Wang [14]). During this process, their thermodynamic structures undergo significant changes (Shen-Ming F et al. [18]; L Wei et al. [19]; Xu et al. [20]; Yan Q et al. [21]). Additionally, the causes of such heavy rainfall are highly complex, and the lack of effective observational data hampers our understanding of the internal structure evolution of the transformed typhoon after merging with the cold vortex. However, the studies on the process of typhoon degeneration and merging into the Northeast Cold Vortex are relatively few and limited to the characterization of meteorological features or the analysis of precipitation causes (Cheng, et al. [22]; Li and Wang [23]; Liang, et al. [24]; Meng and Wang [25,26]), while the changes in the thermodynamic structure of the typhoon before and after its merging into the Northeast Cold Vortex, as well as the physical mechanisms involved, are still not clear. This paper focuses on the evolution of the cyclone into the cold vortex, utilizes high-resolution numerical simulation data to conduct a detailed diagnostic analysis of the thermodynamic structure changes during the typical typhoon "Maysak" merging with the Northeast Cold Vortex and the associated strong precipitation process. It aims to summarize a typical physical conceptual model, in order to enhance the understanding of the mechanisms behind typhoons merging with cold vortices and their strong precipitation processes and to improve the forecasting service capabilities for typhoon prevention and disaster mitigation.

2. High-Resolution Numerical Simulation and Validation

This paper selected Typhoon "Maysak" (Typhoon No. 9 of 2020) as a case study for a high-resolution numerical simulation. "Maysak" formed over the ocean east of the Philippines on 28 August (see Figure 1), intensified into a super typhoon on 31 August at 21:00 UTC, with the strongest winds near its center reaching super typhoon level (52 m per second), and made landfall along the coast of Busan, South Gyeongsang Province, South Korea around 17:30 UTC on September 2nd (42 m per second, strong typhoon level); it entered Yanji City, Yanbian Korean Autonomous Prefecture, Jilin Province, China around 05:40 UTC September 3rd (20 m per second, tropical storm level); around 12:00 UTC on September 3rd, it entered the territory of Wuchang City, Heilongjiang Province (18 m per second, tropical storm level) and transformed into an extratropical cyclone in Lindian County, Heilongjiang Province in the early morning of the 4th, entering Hulun Buir City, Inner Mongolia Autonomous Region around noon, and the Central Meteorological Observatory ceased its numbering around 09:00 UTC on 4 September. "Maysak" lasted for 8 days from its formation to its transformation into an extratropical cyclone in the northeastern region of China until it was de-registered. Although "Maysak" entered the northeastern region of China after its intensity weakened, its combination with the cold air allowed it to maintain its strength for a long time, resulting in a broad and prolonged

impact from wind and rain. The center of "Maysak" was over Chinese territory for as long as 27 h, and its influence in terms of wind and rain lasted for about 45 h.

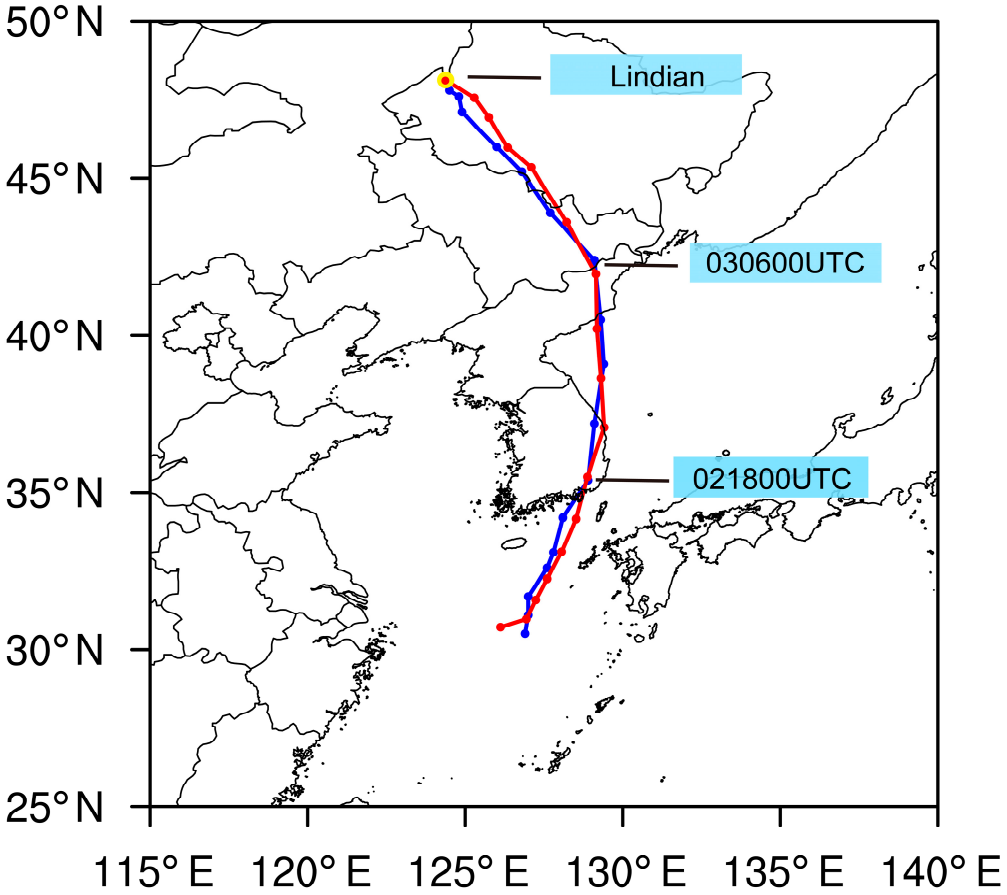

Figure 1. The actual path of Typhoon "Maysak" (red line) and the simulated path (blue line).

This study utilized the mesoscale numerical model WRF V4.2 to simulate the process. The input background field data were the FNL data from the National Centers for Environmental Prediction (NCEP), with a resolution of 1° × 1° and a temporal interval of 6 h, available at UCAR Research Data Archive (https://rda.ucar.edu/datasets/ds083-2/ (accessed on 13 January 2024.)). The observed typhoon data were sourced from the Best Track Data Set provided by the Tropical Cyclone Data Center of the China Meteorological Administration. This data set includes the typhoon center location, tropical cyclone category, typhoon central sea level pressure, and the maximum near-surface wind speed, with a temporal interval of 3 h. The observed precipitation data were derived from station data of the China Meteorological Administration. The model initiation time was 00:00 UTC on 2 September 2020, with the simulation ending at 00:00 UTC on 4 September 2020. A single-level nested simulation was employed, with the model's horizontal resolution set at 3 km × 3 km, consisting of a 901 × 901 grid-point configuration. The simulation domain selection is shown in Figure 2a. There were 81 vertical layers, with the model top height at 50 hPa, and the integration time step was 10 s. The microphysical process scheme was the Thompson scheme (Thompson et al. [27]), the shortwave radiation scheme was the Dudhia scheme (Dudhia [28]), the longwave radiation scheme was the RRTM scheme (Mlawer et al. [29]), the land surface process employed the Noah scheme (Niu et al. [30]), and the boundary layer scheme was the YSU scheme (Hong et al. [31]). Given the high horizontal resolution of the model, no cumulus convection parameterization scheme was used.

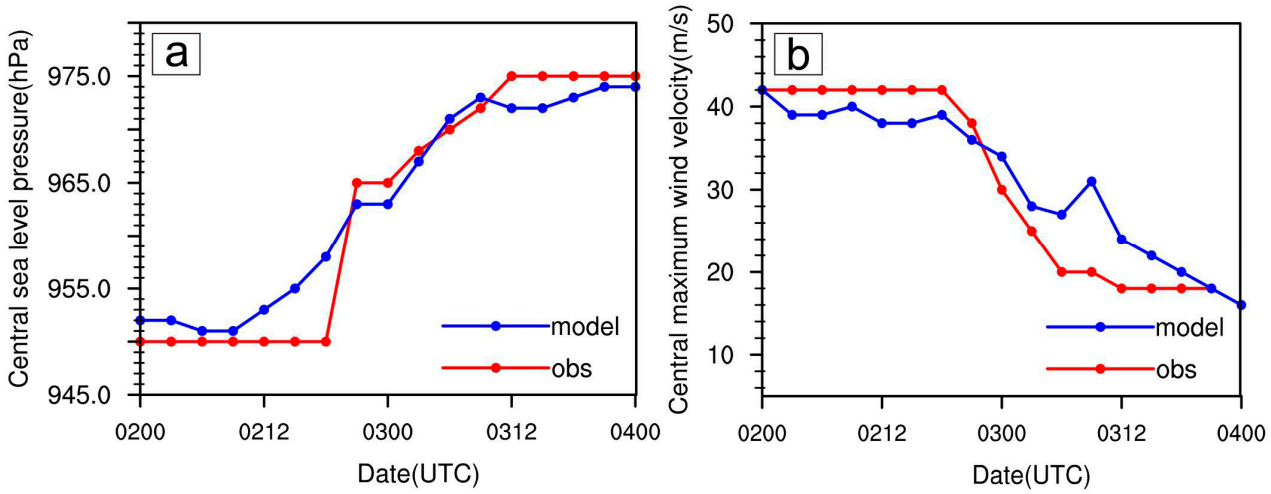

Figure 2. Typhoon "Maysak": (**a**) the observed central sea level pressure (red line) and the simulated central sea level pressure (blue line); (**b**) the observed maximum wind speed near the center (red line) and the simulated maximum wind speed near the center (blue line).

Figure 1 presents the simulated (blue line) and observed (red line) tracks of Typhoon "Maysak". Compared to the observed track, except for a slight eastward bias at the initial moment, the simulated track of "Maysak" from 00:00 UTC on 2 September 2020 to 00:00 UTC on 4 September was essentially consistent with the actual situation. The simulated path and observation were in basic agreement, with the simulated typhoon path being slightly westward after the typhoon's entry into China compared to the observation, but the direction was consistent with minimal error. As can be seen from the figure, around 05:40 UTC on 3 September, "Maysak" began to move into Jilin Province, China, and started to move northwestward. Both the turning point and the time of turning were well simulated and consistent with the actual situation. It entered the territory of Wuchang City, Heilongjiang Province, around 12:00 UTC on the 3rd, then continued to move northwestward and gradually transformed into an extratropical cyclone. From the night of the 2nd to the morning of the 3rd, as the typhoon crossed the Korean Peninsula and continued to move northward, approaching the eastern part of Jilin Province in China, the typhoon's trough had already begun to affect the eastern part of Jilin. During this stage, the typhoon exhibited a dense overall circulation but started to show asymmetric structure. A closed low-pressure center existed over the southern part of Northeast China to the northeastern part of North China, with the typhoon and the westerly belt system being independent of each other. At this stage, convective precipitation occurred in the eastern part of Jilin. Before the typhoon made landfall in China (around 06 UTC on the 3rd), the two independent low-value centers merged into one, indicating a trend of combination between the typhoon and the westerly belt system at high altitudes. Starting in the afternoon of the 3rd, as the main body of the typhoon entered China and gradually combined with the westerly belt system, the asymmetry of the typhoon's structure further intensified.

The comparison between the simulated and observed central sea level pressure changes and the maximum wind speed near the center of Typhoon "Maysak" is shown in Figure 2. As can be seen from the figure, the trends of the central sea level pressure changes of the simulated and observed typhoon were quite consistent. The model well reproduced the process of changes in the central sea level pressure and the maximum wind speed near the center of Typhoon "Maysak" after it moved into Jilin Province, China. During the simulation period, the changes in the typhoon's lowest pressure and maximum wind speed were relatively small. The lowest pressure increased from 950 hPa to 975 hPa, and the maximum wind speed decreased from 40 m/s to 20 m/s. The overall trend of the simulation was in good agreement with the actual situation, effectively reflecting the process of "Maysak" gradually weakening and maintaining itself for a long time in the northeastern

region of China. Overall, the model successfully captured the characteristics of the path and intensity changes in the development and evolution process of Typhoon "Maysak".

The simulated precipitation was validated using station data from the China Meteorological Administration. It can be seen that the simulated 48 h cumulative precipitation (Figure 3b) corresponded well with the observations (Figure 3a), especially in the south-central part of Jilin Province and the southwestern part of Heilongjiang Province, where areas with cumulative precipitation exceeding 100 mm were well reproduced. Figure 3c,d shows a comparison between the observed infrared cloud image (from the Japan Meteorological Agency) and the simulated cloud top temperature at 12:00 UTC on 2 September. It can be observed that both the observed and simulated typhoon centers were located in the southern part of the Korean Peninsula, with the typhoon cloud system extending northward. The simulated and observed typhoon radii were relatively consistent in size. The simulated data effectively reflected the cloud system structure of Typhoon "Maysak".

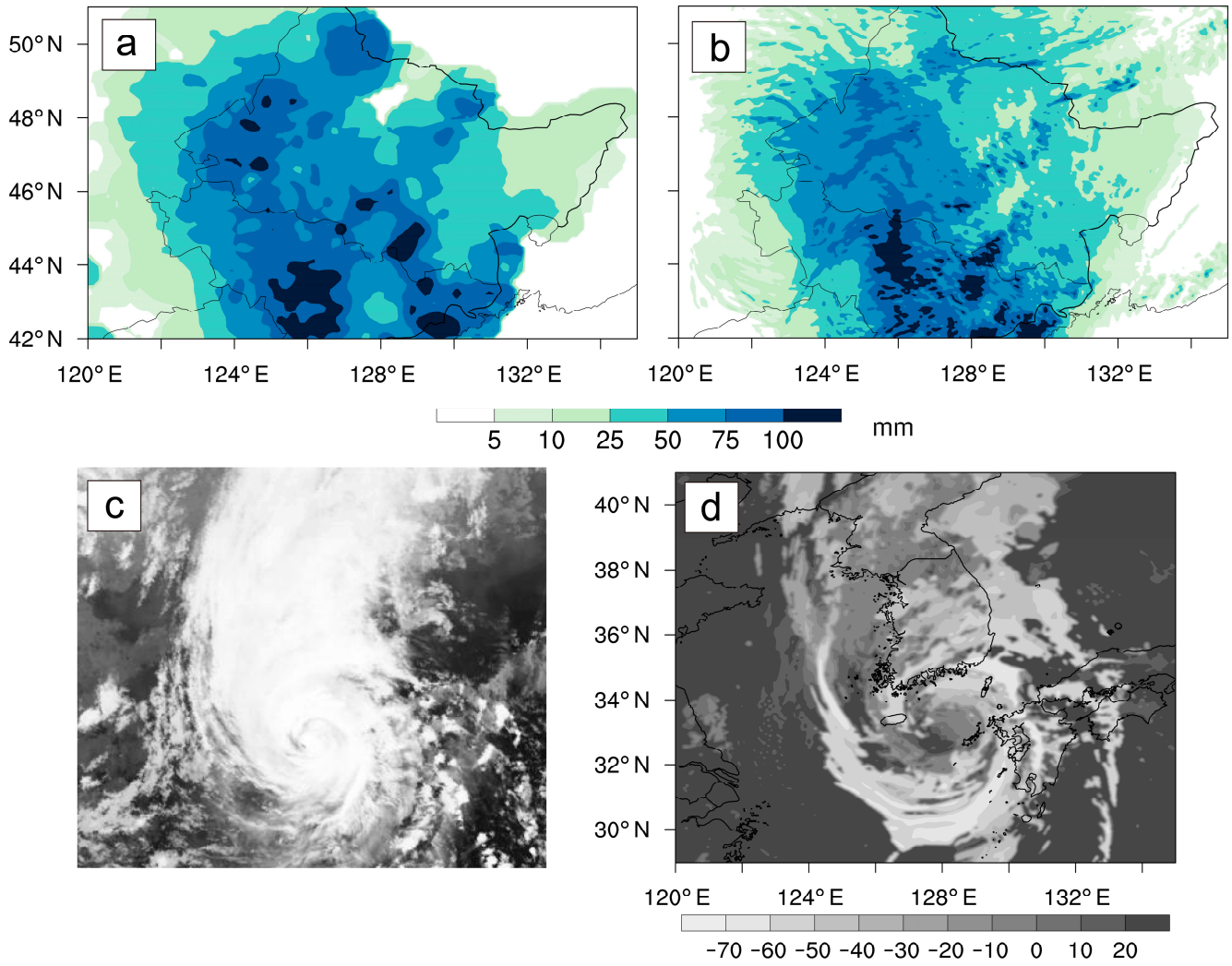

Figure 3. Distributions of (**a**) observed and (**b**) simulated cumulative precipitation (shaded, units: mm) from 00:00 UTC on 2 September to 00:00 UTC on 4 September 2020; and infrared cloud image (**c**) observed at 12:00 on 2 September 2020, (**d**) Simulated cloud top temperature.

3. Diagnostic Analysis

From the large-scale circulation situation field, it can be seen that "Maysak" was jointly influenced by the subtropical high, the high pressure east of the Japan Sea or the Okhotsk Sea high (blocking high), and the cold vortex or trough on the west side of the typhoon (Figure 4). The 500 hPa circulation center of the cold vortex was located near the

northeast region. As the typhoon continued to move northward, the center of the cold vortex circulation and the center of the typhoon rotated counterclockwise and moved closer together. "Maysak" moved northward and merged with a small trough on the southern side of the cold vortex at 12:00 UTC on the 2nd (Figure omitted), and then continued to move northward. During that period, its west side was continuously invaded by cold air brought by the northwesterly wind, while the blocking high on its east side was a warmer southerly wind, causing the temperature gradient direction near "Maysak" to change from northwest–southeast (Figure 4a) to northeast–southwest (Figure 4c). At 18:00 UTC on the 3rd, "Maysak" weakened into a low-pressure system, and its 500 hPa circulation center showed a clear separation from the warm center. At the same time, a strong pseudo-adiabatic potential temperature gradient appeared at the circulation center, that is, the baroclinicity was obvious, indicating that "Maysak" began to gradually transform into an extratropical cyclone (Figure 4c). During the process of merging into the Northeast Cold Vortex, the temperature near the cyclone's circulation center turned colder, and the strength of the cyclone's 500 hPa circulation center intensified, with the geopotential height value dropping from 5520 gpm at 18:00 UTC on the 3rd (Figure 4c) to 5440 gpm at 06:00 UTC on the 4th (Figure 4d). After that, the cyclone slowly moved northward in the Northeast region, maintaining its strength, and did not start to significantly weaken and retreat northward until 12:00 UTC on the 4th.

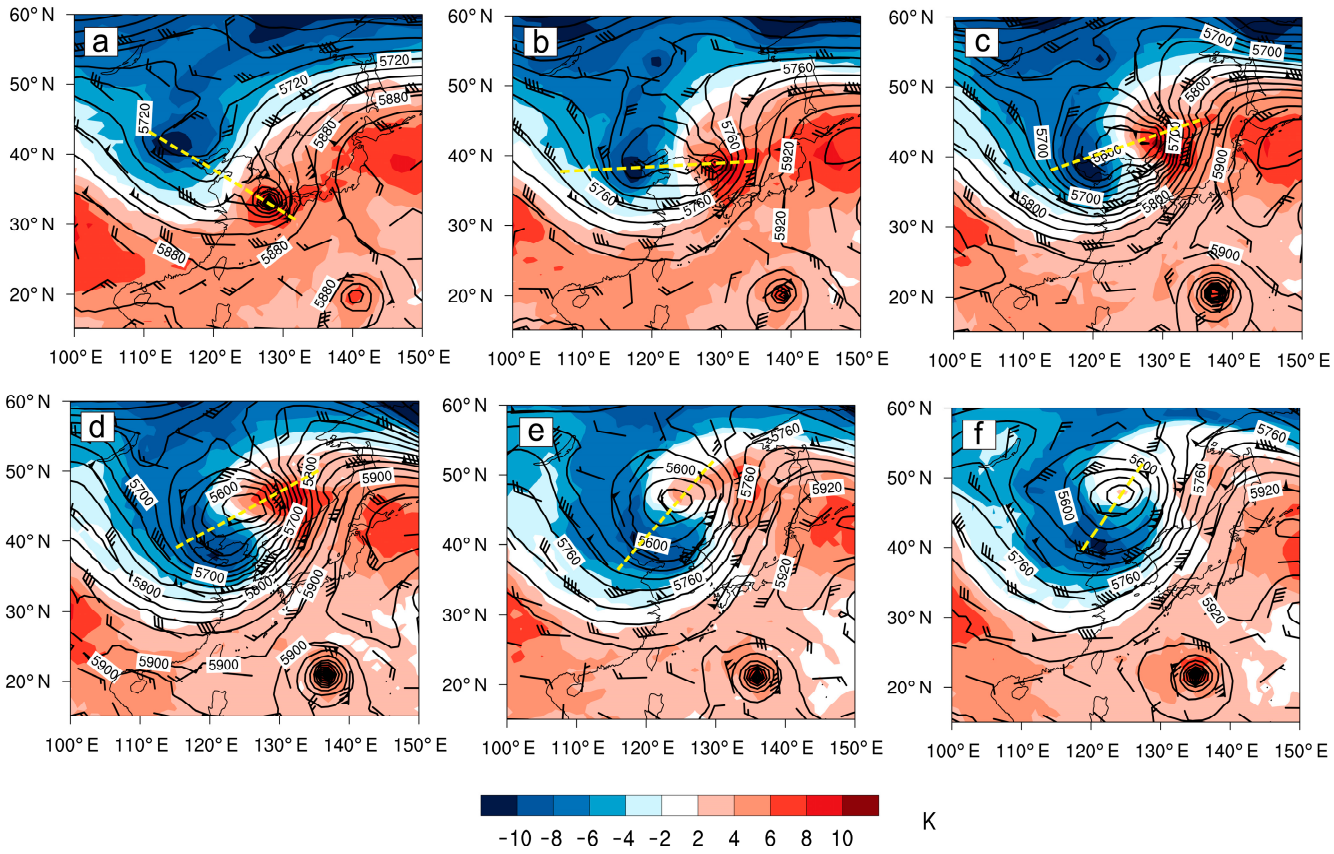

Figure 4. Distribution of 500 hPa geopotential height field, 500 hPa temperature anomaly, and wind vector: (**a**) 12 UTC on the 2nd, (**b**) 00 UTC on the 3rd, (**c**) 06 UTC on the 3rd, (**d**) 12 UTC on the 3rd, (**e**) 18 UTC on the 3rd, (**f**) 00 UTC on 4 September.

The analysis of the configuration and changes of the high and low altitude systems during the process of combining with the westerly belt system (Figure 5) shows that the 500 hPa circulation center merged from two previous vorticity centers into one, and there were two divergence centers at 200 hPa (Figure omitted), located in Heilongjiang and the southern part of Liaoning, respectively. With the combination of the westerly belt system

and the typhoon, the upper layer also gradually merged into one divergence center, which was positioned west of the lower layer convergence area (Figure 5a). Before the interaction between the typhoon and the westerly belt system, the relative vorticity across the typhoon center showed a vertical distribution feature between high and low layers, with the typhoon maintaining a warm core structure, where the warm advection center and the center of the positive temperature anomaly basically coincided (Figure 5b). After the typhoon entered China and interacted with the westerly belt system, the area of high relative vorticity began to tilt westward with increasing height (Figure 5c). At that time, although the warm core structure of the typhoon was not destroyed, there was a clear temperature gradient accompanied by cold advection in the lower layer, and a significant frontogenesis process occurred, with precipitation showing a significant asymmetric distribution (Figure 5d).

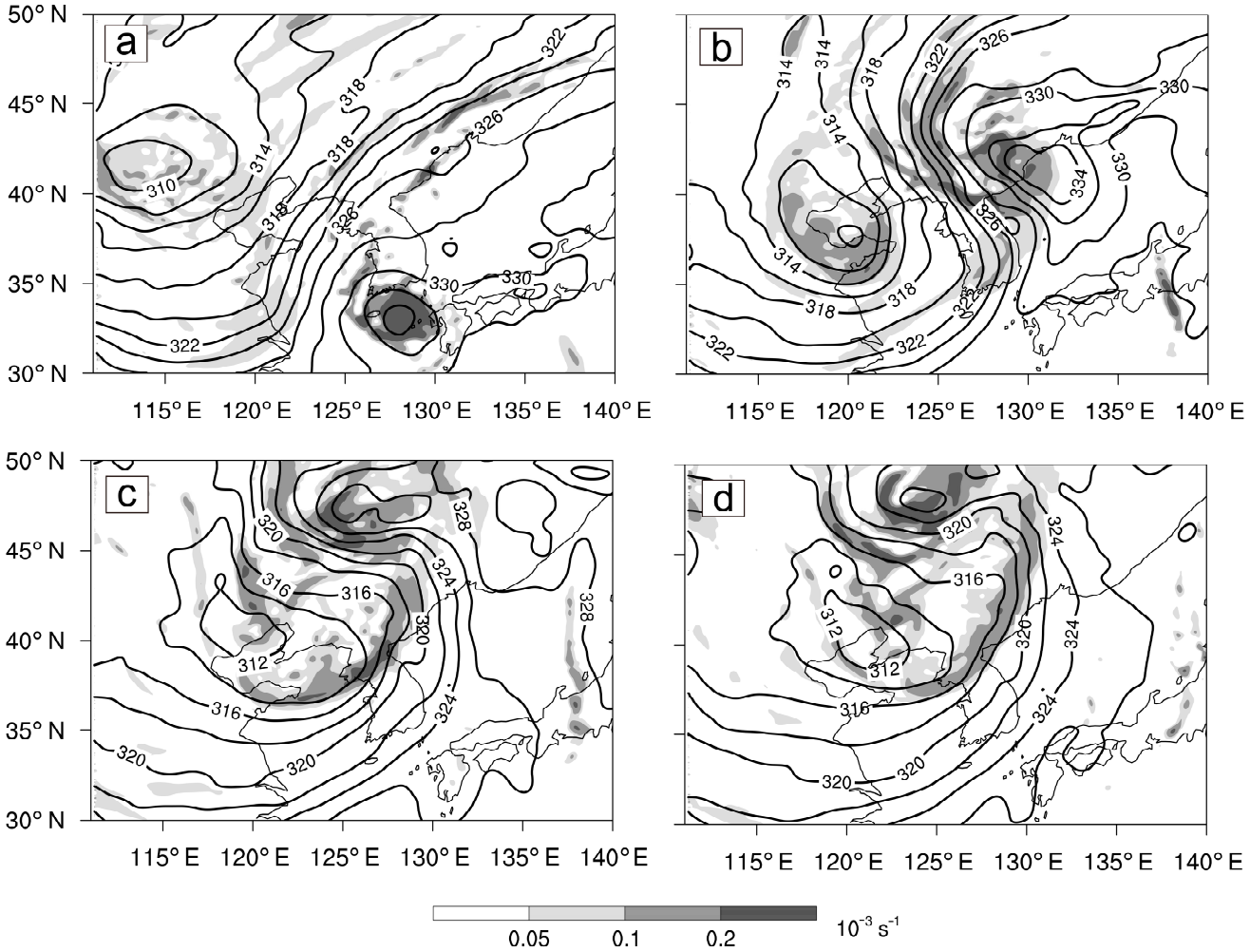

Figure 5. Interval of 6 h (**a**–**d**) vertical vorticity (color-filled, unit: 10^{-3} s^{-1}) and pseudo-adiabatic potential temperature (contour lines, unit: K) at 500 hPa: (**a**) 12 UTC on 2 September, (**b**) 06 UTC on 3 September, (**c**) 18 UTC on 3 September, (**d**) 00 UTC on 4 September.

Figure 6 illustrates the evolution of the vertical profile of temperature departures and geopotential height departures along the line connecting the centers of the Northeast Cold Vortex and Maysak. Before the typhoon merged with the Northeast Cold Vortex (Figure 6a), both the typhoon and the cold vortex largely maintained their distinct structural characteristics: the typhoon exhibited a pronounced warm core structure at high altitudes, with the warm center near 350 hPa, with a corresponding configuration of low pressure at low levels and high pressure at high levels, where the high-level high pressure was directly caused by the high-altitude warm core (based on the relationship of the atmospheric state

equation), and the low-level low pressure was related to the upper-level high pressure forming a high-altitude divergence that sucked in low-level air; the Northeast Cold Vortex showed a distinct high-altitude cold vortex characteristic, that is, a high-altitude cold core and a high-altitude low-pressure center configuration, with the low-pressure center located between 150 and 200 hPa. When the typhoon transformed into an extratropical cyclone and merged with the Northeast Cold Vortex, its warm core structure gradually died out (Figure 6b–d), and after moving into the Northeast Cold Vortex, it turned into a whole-layer cold bias, with a cold center appearing at low levels (Figure 6d). The demise of the warm core structure led to a significant weakening of the high-level divergence and low-level convergence, and the low-level low-pressure center disappeared accordingly (Figure 6b–d). The distribution of low-level low pressure and high-level high pressure gradually turned into a whole-layer low-pressure distribution, where the low-pressure center first appeared at mid-low levels (700–900 hPa), and the low pressure was distributed in a tilting connection with the high-altitude cold vortex (Figure 6d). This indicates that during the process of merging with the Northeast Cold Vortex, the intensity of the extratropical cyclone was maintained, which was conducive to the occurrence of large-area heavy precipitation in the northeast region at that time. At the same time, as the cyclone merged with the Northeast Cold Vortex, the temperature of the mid-low levels of the cold vortex increased significantly, and correspondingly, the low-pressure strength at the mid-low levels of the cold vortex weakened, that is, the characteristics of the cold low pressure weakened, and at the same time, the Northeast Cold Vortex retreated northward.

Figure 7 shows the distribution of potential vorticity and pseudo-adiabatic potential temperature along the cross-section of the line connecting the centers of the Northeast Cold Vortex and Maysak. One of the main reasons for the long-term maintenance after the typhoon's landing was the replenishment of positive vorticity obtained from the baroclinic zone of the environmental field in the upper layers of the typhoon. The cross-sectional diagrams of the vorticity before and after the two landfalls of "Maysak" were analyzed (Figure 7). On 2 September at 12 UTC (Figure 7a), the typhoon showed a clear symmetrical structure with the center of maximum vorticity near 850 hPa, at 9.0×10^{-4} s^{-1}. At 02 on 3 September (Figure omitted), after landing, the intensity of the typhoon weakened rapidly, and the center of maximum vorticity in the lower layer decreased to about 6.0×10^{-4} s^{-1}. After that, as the typhoon re-entered the sea, before the second landing at 00 UTC on 3 September, the vorticity center at 850 hPa further weakened, while the vorticity at around 400 hPa in the middle layer strengthened, showing a large value center of about 5.0×10^{-4} s^{-1}. This was due to the long-wave trough at 500 hPa merging with the typhoon, and the positive vorticity advection in front of the trough supplied the middle layer of the typhoon with a replenishment of positive vorticity. At 06 UTC on 3 September, after the second landing (Figure 7b), the deep symmetrical structure of the typhoon turned into an asymmetrical structure, the center of positive vorticity in the upper layer disappeared, the center of positive vorticity in the lower layer weakened, and the stretching height of the positive vorticity area decreased to about 300 hPa. In the following 24 h (from 06 UTC on 3 September to 06 UTC on 4 September), the positive vorticity between 200 and 400 hPa in the upper layer was maintained and slightly strengthened, while the positive vorticity center at 850 hPa in the lower layer first strengthened and then weakened. After 12 UTC on 4 September, the stretching height of positive vorticity in the vertical direction gradually decreased, and the intensity significantly weakened. In addition, the southwest wind in front of the upper-level cold vortex trough and the northeast wind on the north side of the upper layer of the typhoon brought obvious warm advection, which was distributed obliquely from the north side of the upper layer of the typhoon to the front of the high-altitude cold vortex trough, causing the warm area in the upper layer of the typhoon to tilt towards the high-altitude cold vortex (Figure 7a,b). After the typhoon transformed and merged into the Northeast Cold Vortex, the whole layer turned cold, a cold center was formed at low levels, and the temperature advection obviously weakened. At the same time, affected by the obvious warm advection brought by the north wind on the north side

of the middle and low layers of the cyclone after transformation, the middle and low layers of the Northeast Cold Vortex increased in temperature, and the cold heart characteristics of the cold vortex in the middle and low layers weakened (Figure 7c,d).

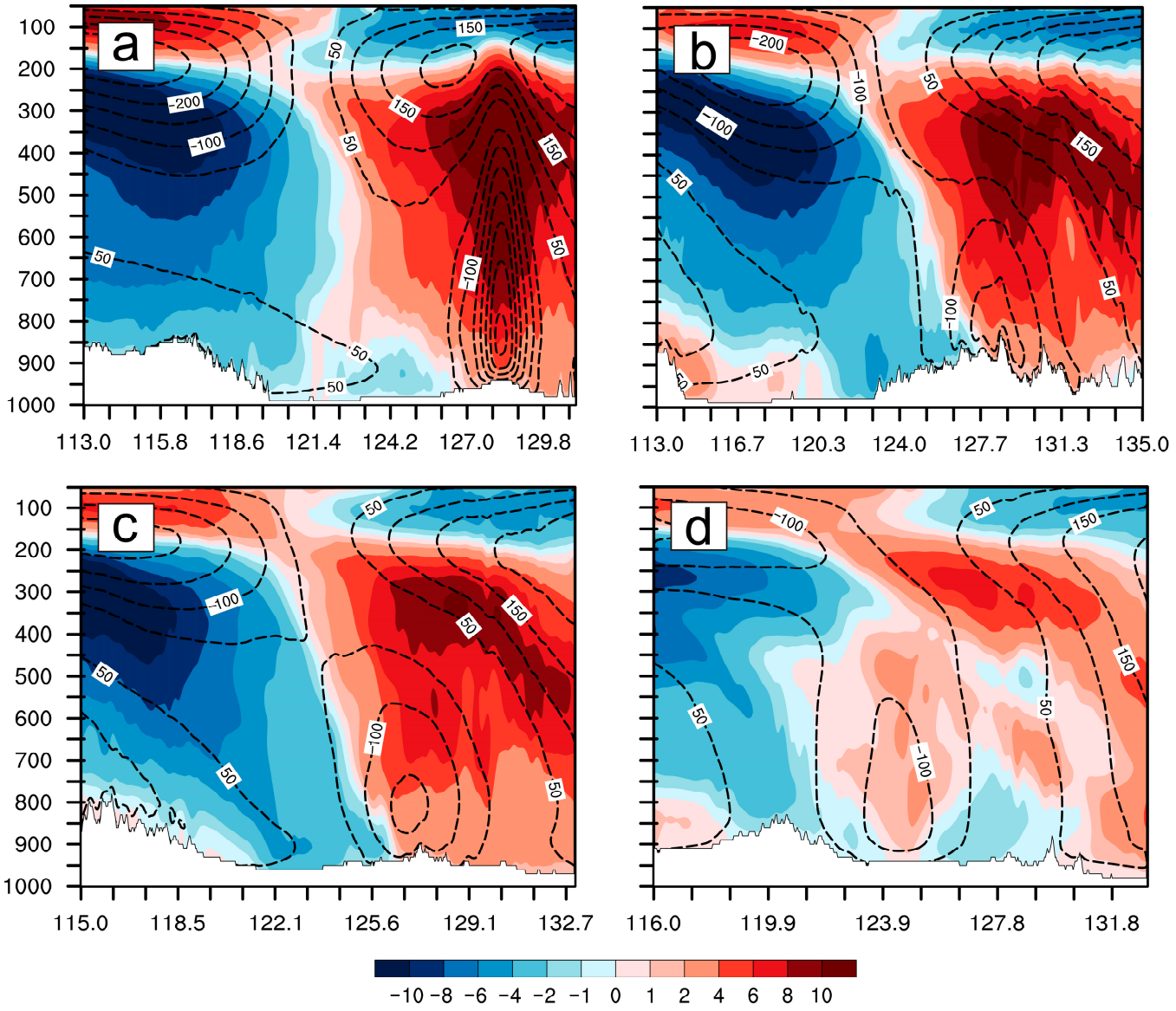

Figure 6. Evolution of the vertical profile of the temperature anomaly and geopotential height anomaly along the line connecting the centers of the Northeast Cold Vortex and Maysak, as indicated by line AB in Figure 1: (**a**) 00 UTC on 2 September, (**b**) 06 UTC on 3 September, (**c**) 12 UTC on 3 September, (**d**) 00 UTC on 4 September.

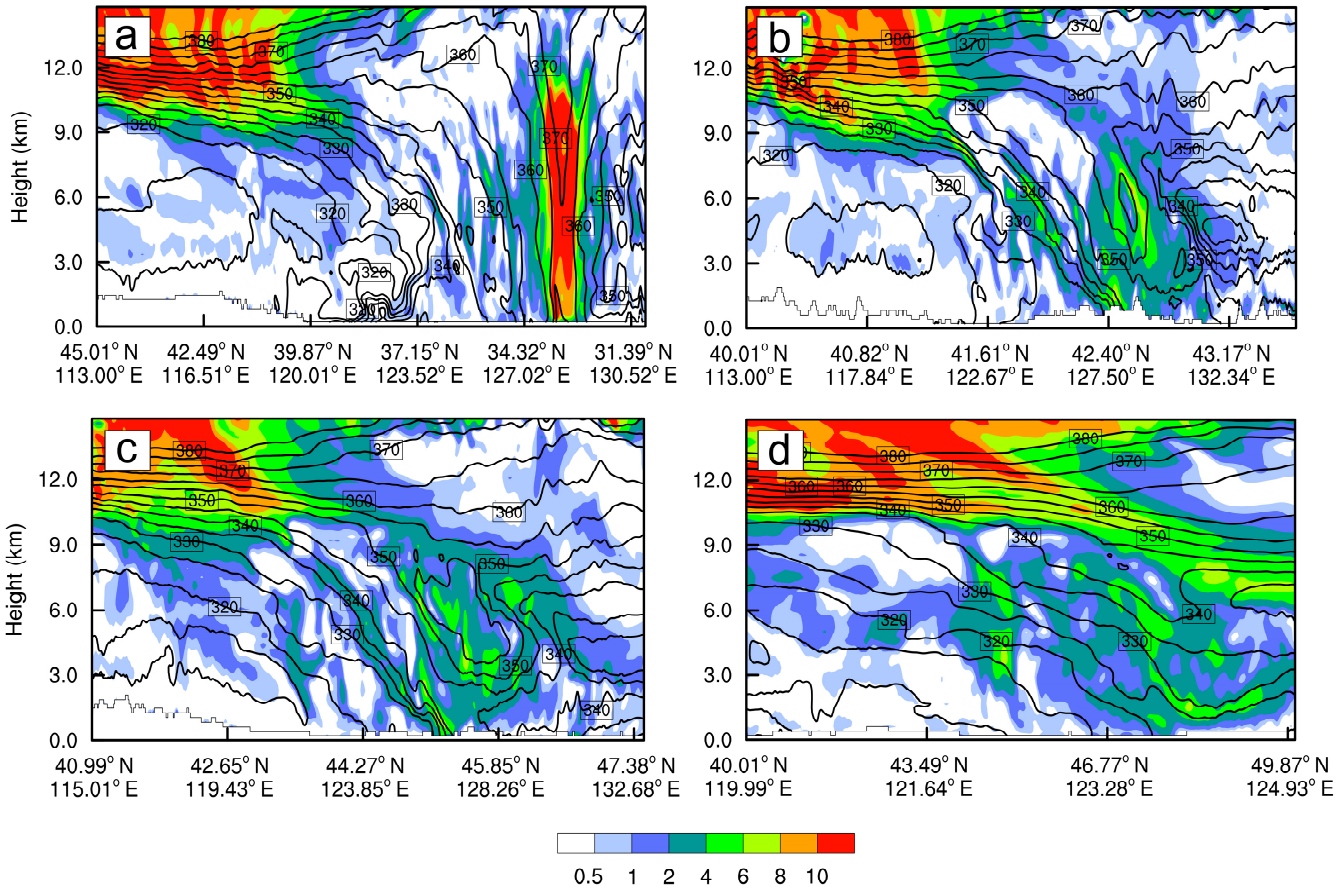

Figure 7. Distribution of potential vorticity and pseudo-adiabatic potential temperature along the cross-section of the line connecting the Northeast Cold Vortex and Maysak's center: (**a**) 12 UTC on 2 September, (**b**) 06 UTC on 3 September, (**c**) 12 UTC on 3 September, (**d**) 00 UTC on 4 September.

Figure 8 illustrates that the distribution and evolution of the vertical vorticity of Maysak can be roughly divided into three stages: before the typhoon transformed and merged with the Northeast Cold Vortex (before 00:00 UTC on the 2nd, Figure 8a), the entire layer exhibited strong vertical vorticity (basically greater than 2×10^{-4} s^{-1}), with the strong vertical vorticity area mainly concentrated in the upper layer (the area greater than 4×10^{-4} s^{-1} is primarily located between 200 and 400 hPa). Around 00:00 UTC on the 3rd, the strong vertical vorticity expanded to lower altitudes, and the vertical vorticity near the upper cold vortex increased (Figure 8b); when the typhoon was transforming and merging with the Northeast Cold Vortex (Figure 8c), the vertical vorticity of the entire layer first rapidly weakened significantly, then the vertical vorticity in the middle and lower layers strengthened; after the typhoon transformed and merged with the Northeast Cold Vortex (after 00:00 UTC on the 4th, Figure 8d), the vertical vorticity in the middle and lower layers was maintained, and the vertical vorticity in the upper layer was significantly enhanced, with the entire layer showing strong vertical vorticity (basically greater than 1×10^{-4} s^{-1}). It can be seen that the maintenance of the intensity of the middle and lower layers of the typhoon before it merged with the Northeast Cold Vortex was mainly due to its own action, and the merging with the westerly trough played a certain role in promotion. During the process of the typhoon transforming and merging with the Northeast Cold Vortex, the movement of its circulation kept the jet axis of the upper cold vortex periphery tilted, and the thermodynamic distribution characteristics on the left side of the tilted jet axis were conducive to the development of vertical vorticity, thus promoting the cyclone to tilt and develop towards the upper cold vortex. After the cyclone merged with the Northeast Cold

Vortex, the positive vertical vorticity advection on the periphery of the upper cold vortex made the cyclone rapidly develop towards the upper altitudes.

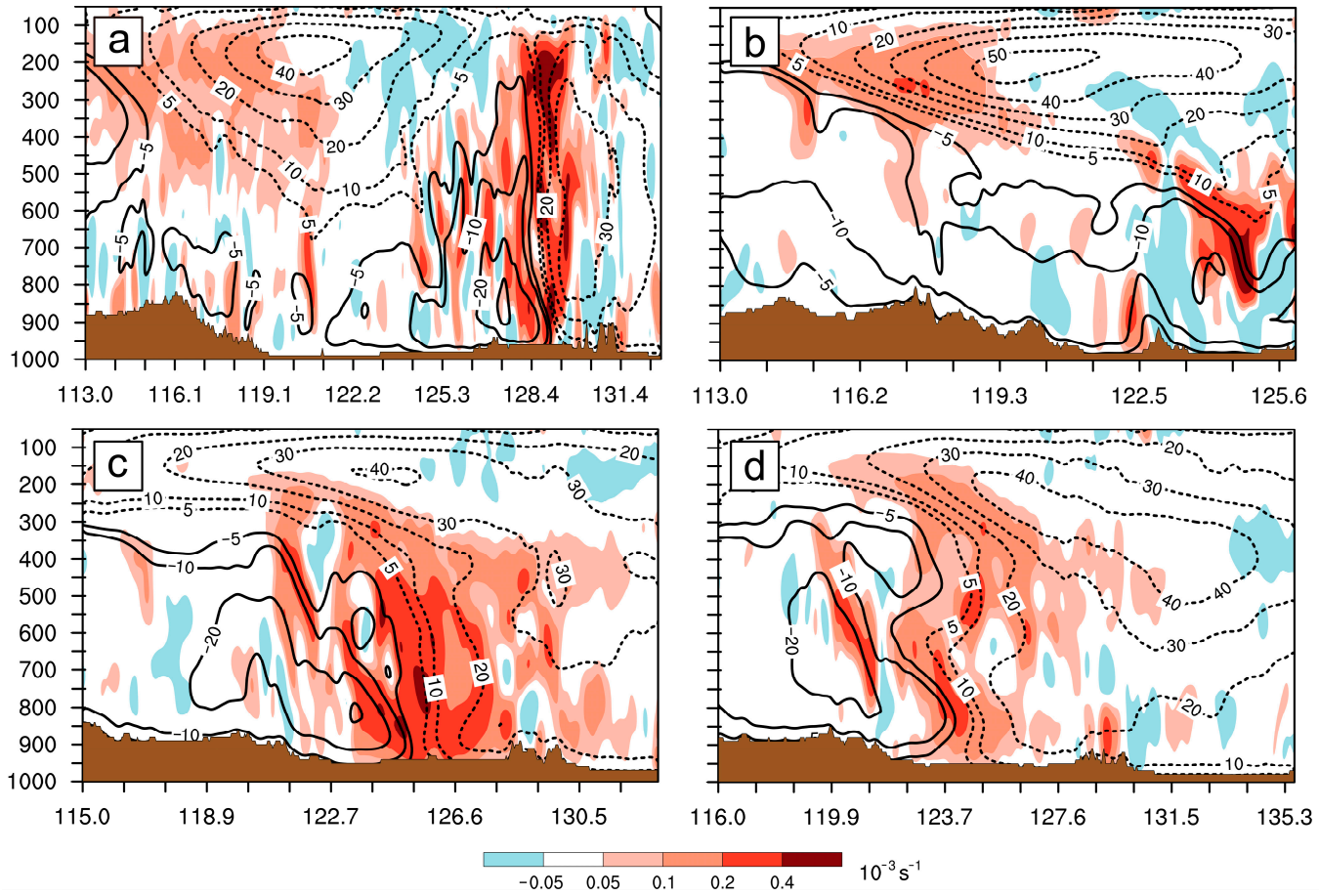

Figure 8. Distribution of vertical vorticity (color-filled, unit: 10^{-3} s^{-1}) and normal wind (dashed and bold lines, unit: $m \cdot s^{-1}$) along the cross-section of the line connecting the Northeast Cold Vortex and Maysak's center: (**a**) 00 UTC on 2 September, (**b**) 00 UTC on 3 September, (**c**) 18 UTC on 3 September, (**d**) 00 UTC on 4 September.

Incorporating the spatiotemporal distribution characteristics of precipitation, an analysis of the evolution of accumulated precipitation over 6 h was conducted (Figure 9). The convergence areas to the north and west of the typhoon center had strong precipitation, mainly affecting the central and eastern parts of Jilin and the southeastern part of Heilongjiang (Figure 9a,b). After the typhoon combined with the westerly belt system, strong precipitation occurred successively in the central and western parts of Jilin, the southern and western parts of Heilongjiang, and other places. The precipitation at that time was mainly frontal, with greater intensity and a larger range than the earlier period (Figure 9c,d). During the interaction between "Maysak" and the westerly belt system from the afternoon to the night of the 3rd, the precipitation intensity was the strongest, and the asymmetrical characteristics were the most pronounced (Figure 9e,f).

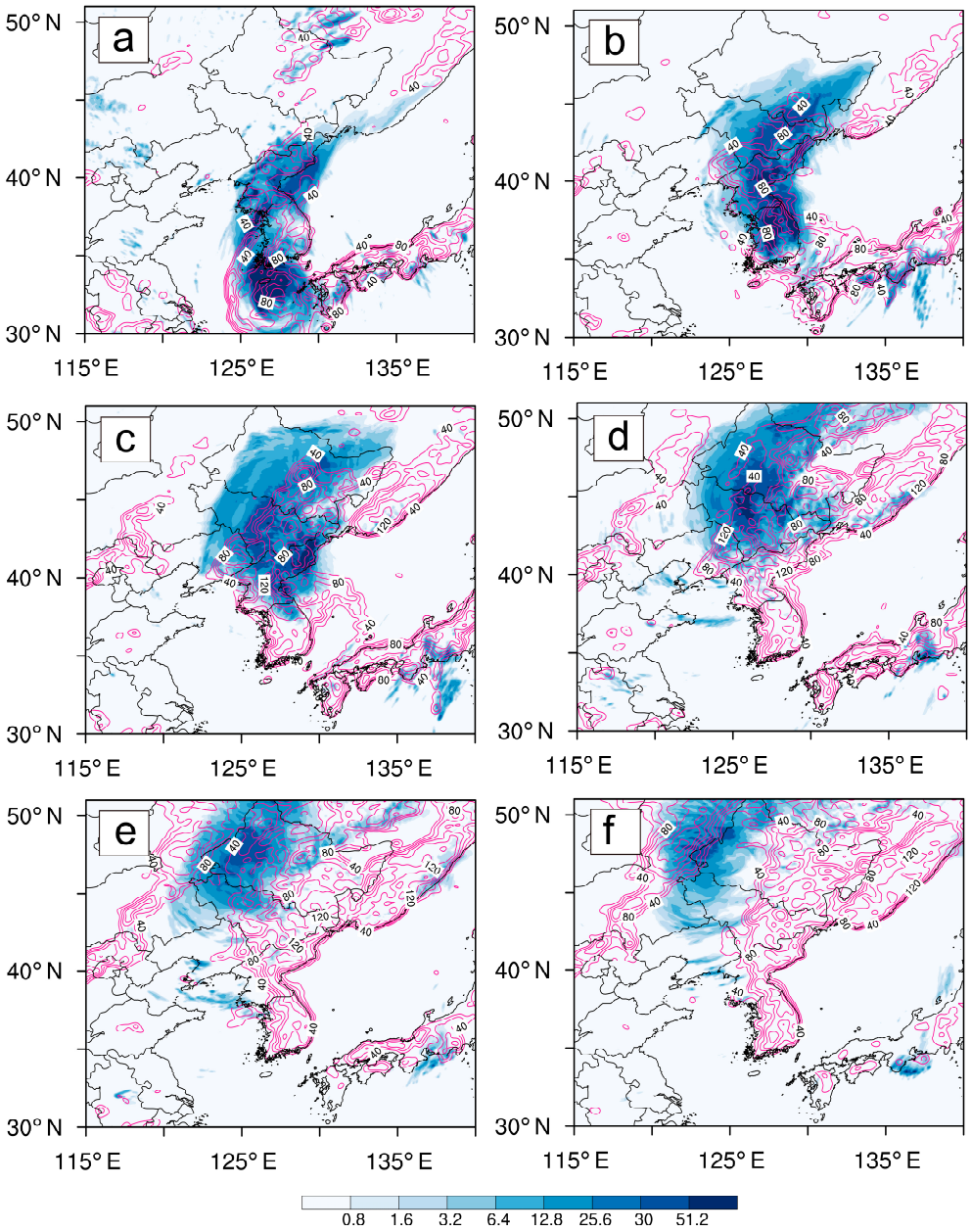

Figure 9. Horizontal distribution of the thermodynamic shear vorticity parameter (shaded area) and simulated accumulated precipitation over 6 h: (**a**) 12 UTC on 2nd, (**b**) 00 UTC on 3rd, (**c**) 06 UTC on 3rd, (**d**) 12 UTC on 3rd, (**e**) 18 UTC on 3rd, (**f**) 00 UTC on 4 September.

The thermodynamic shear vorticity parameter characterizes the development and evolution of precipitation systems by combining the vertical component of the convective vorticity vector, horizontal divergence, and the vertical gradient of the generalized potential temperature (Wang et al. [32]). The vertical integral of the moist thermodynamic advection parameter $\boldsymbol{J}$ can be written as:

$$J = \int_{850}^{500} \rho |\nabla_h(-V \cdot \nabla\theta) \cdot \nabla_h \theta *| \mathrm{d}p$$

Among them, ∇h represents the horizontal gradient operator, ∇ denotes the three-dimensional spatial gradient operator, ρ signifies density, θ indicates the potential tempera-

ture, $\boldsymbol{\theta}^*$ stands for the pseudo-adiabatic potential temperature, p is the air pressure, and $\boldsymbol{V}$ = (u, v, ω) is the three-dimensional velocity vector in an isobaric coordinate system.

This parameter $\boldsymbol{J}$ can comprehensively represent the kinematic and thermodynamic characteristics of the horizontal wind field shear above the rain area and the funnel-shaped downward extension of the moist isentropic surface. It is closely related to the development and evolution of the precipitation system and has a certain correspondence with the simulated accumulated ground precipitation area over 6 h. In terms of spatial horizontal distribution and trend evolution, the anomaly area of the thermodynamic shear vorticity parameter basically covers the simulated accumulated ground precipitation area over 6 h (Figure 9). The results showed that throughout the research period, the anomaly area of the perturbation thermodynamic divergence parameter was always covered above the ground rain area. The spatial distribution and temporal evolution trend of the two were relatively consistent, and the perturbation thermodynamic divergence parameter showed a strong signal in the precipitation area, while it showed a weak signal in the non-precipitation area. The perturbation thermodynamic divergence parameter had a good indicative effect on the area of heavy precipitation. The high-value center of J did not completely coincide with the center of precipitation, being primarily located on the edge of the precipitation center; its gradient high-value area, however, corresponded to the center of precipitation. This is consistent with the conclusion drawn from the previous analysis of the thermodynamic advection parameter and the accumulated ground precipitation center over 6 h. Additionally, some weak precipitation areas did not have a corresponding J value, which also illustrates the insufficiency of the thermodynamic advection parameter in tracing weak precipitation.

4. Results

In the process of Typhoon Maysak moving closer and degenerating into the Northeast Cold Vortex (Figure 10), the warm advection at high altitude in front of the cold vortex trough and north of the upper level of the typhoon caused the warm area of the typhoon's high altitude to tilt toward the front of the cold vortex trough at high altitude. The cold air at the bottom of the northeast cold vortex trough invaded the typhoon continuously from the middle and lower levels to the whole level, the relative cold advection generated by the typhoon movement made the warm core structure of the typhoon gradually die out, and its dynamic structure of low-level low-pressure convergence and high-pressure dispersion at the upper level subsequently disappeared.

From the viewpoint of the upper-level outflow conditions: Typhoon Maysak was in the strong dispersion zone to the right of the entrance of the subtropical westerly jet stream, which influenced the strong jet stream of Typhoon Maysak, with the core strength of the 200 hPa jet stream up to 90 m/s, which is rare. It was found that the upper-level outflow conditions of Maysak were good, which was conducive to the maintenance of Maysak's intensity and the development of convection. On the one hand, the cyclone was located on the anticyclonic shear side of the high-altitude cold vortex peripheral rapid, which was not conducive to its direct development to high altitude. On the other hand, the characteristics of the thermodynamic distribution on the left side of the outer rapids' axis of the high-altitude cold vortex were favorable to the development of vertical vorticity, and the approach of the densified cyclonic circulation to the Northeast Cold Vortex was favorable to the maintenance of the tilted outer rapids' axis of the high-altitude cold vortex, thus causing the development of cyclones tilted to the high-altitude cold vortex.

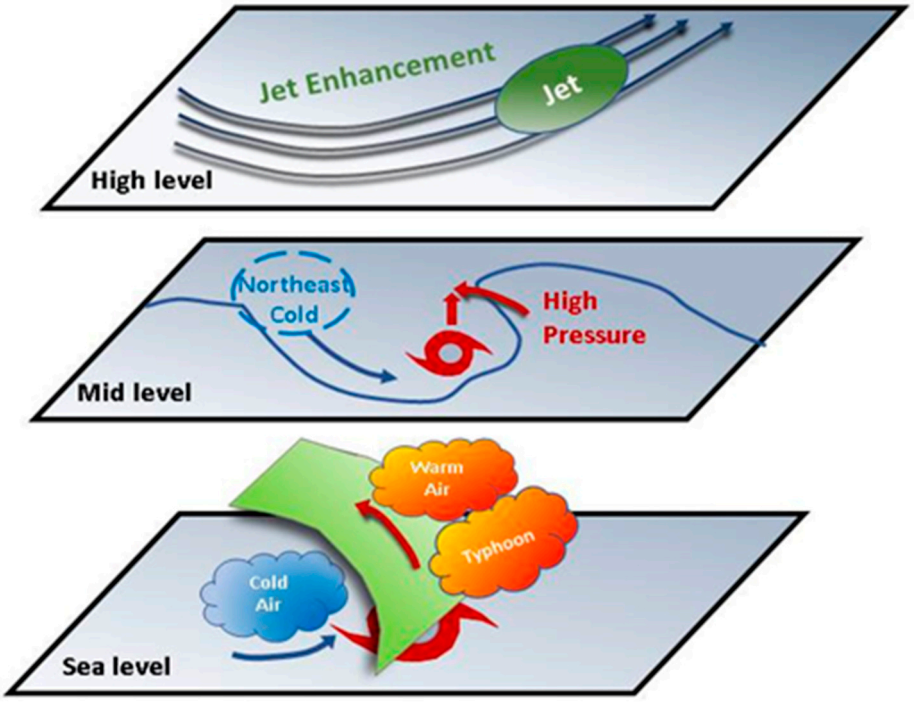

Figure 10. Physical concept of Maysak merging into the Northeast Cold Vortex.

From the perspective of the mid- and high-latitude systems in the middle layer: the eastern side of the typhoon was controlled by the blocking high, which influenced the strong eastern blocking of Maysak, and there was an obvious warm advection on its northwest side, resulting in the continuous redevelopment of the blocking high, was is conducive to the maintenance of the warm core structure of Maysak and the strengthening of the high-altitude westerly rapids. This further enhanced the upper-level outflow and helped maintain the typhoon intensity over land. At the same time, there was an obvious cold vortex upstream or west of Maysak, and the dry and cold air in the middle and high latitudes was involved, stabilizing the eastward obstruction, and the pseudo-equivalent temperature contours were densely tilted, which was conducive to the densification and strengthening of the typhoon after merging with the cold vortex. After the typhoon degenerated into a temperate cyclone and merged into the Northeast Cold Vortex, the positive vertical vorticity advection at the bottom of the high-altitude cold vortex trough promoted the direct development of the cyclone to high altitude, while the rapid flow at the bottom of the high-altitude cold vortex trough to the east facilitated the continuous formation of positive vertical vorticity in the high-altitude advection. The development of cyclonic circulation to high altitude led to the weakening of the upper circulation of the Northeast Cold Vortex and the northward withdrawal of the center of the high-altitude cold vortex.

From the ground system development: Typhoon Maysak maintained a period of typhoon structure, the western side of the cold vortex of the low-level cold air slowly invaded, the upper and middle typhoon warm air mass along the cold air upward climbed and combined with the temperate cyclone over the partial warm air mass, the cold and warm air converged, the front strengthened, and the typhoon gradually denatured into a temperate cyclone, in favor of the typhoon and cold vortex merging strengthening.

5. Conclusions and Discussion

The Northeast Cold Vortex is one of the major weather systems in Northeast China in summer, and when a typhoon interacts with the Northeast Cold Vortex, it may lead to widespread heavy precipitation. In this paper, we analyzed the characteristics of the thermal structure of Typhoon Maysak during its transformation into and merging with

the Northeast Cold Vortex, using high-resolution numerical simulation data from the WRF model.

In the process of the typhoon approaching and merging into the Northeast Cold Vortex, the warm core structure of the typhoon gradually disappeared due to the warm air flow and cold vortex trough at the upper level, and the low-pressure convergence at the lower level and high-pressure divergence at the upper level also disappeared. During the transformation and merging of the typhoon into the Northeast Cold Vortex, the motion of its circulation maintained the tilting of the rapids' axis around the upper-level cold vortex, which favored the development of vertical vorticity and promoted the tilting and development of the cyclone toward the upper-level cold vortex. The thermal shear vorticity parameter was able to characterize the typical vertical structure of the kinetic–thermal field above the rain area during the heavy precipitation process and somewhat corresponded with the development and movement of the surface precipitation area.

However, the heavy precipitation process is a complex cloud microphysical process, while the thermal shear vorticity parameter describes the macroscopic kinetic and thermodynamic processes, and the two are not directly linked but are linked through a third party. In this paper, we analyzed a typical case of Typhoon Maysak merging with the Northeast Cold Vortex, aiming to improve the understanding of the mechanism of a typhoon merging with a cold vortex and its heavy precipitation process and to improve the forecasting service capability for typhoon prevention and disaster mitigation.

Author Contributions: Conceptualization, G.Z. and H.D.; methodology, G.Z.; software, H.D.; validation, G.Z. and H.D.; formal analysis, G.Z.; investigation, G.Z.; resources, H.D.; data curation, H.D.; writing—original draft preparation, H.D.; writing—review and editing, G.Z.; visualization, H.D.; supervision, G.Z.; project administration, G.Z.; funding acquisition, G.Z. All authors have read and agreed to the published version of the manuscript.

Funding: This research was funded by National Key Research and Development Program of China grant number 2023YFB3907701, National Natural Science Foundation of China grant number 42375010, CMA Innovation and Development Project grant number CXFZ2023J015, and National Natural Sciences Foundations of China grant number 41405049.

Institutional Review Board Statement: Not applicable.

Informed Consent Statement: Not applicable.

Data Availability Statement: The data presented in this study are available on request from the corresponding author. The data are not publicly available due to privacy.

Conflicts of Interest: The authors declare no conflict of interest.

References

1. Zheng, X.; Zhang, T.; Bai, R. *Rainstorm in Northeast China*; China Meteorological Press: Beijing, China, 1992; pp. 129–138. (In Chinese)
2. Sun, L.; Zheng, X.; Wang, Q. The climatological characteristics of Northeast cold vortex in China. *Q. J. Appl. Meteorol.* **1994**, *5*, 297–303. (In Chinese)
3. Sun, L. A study of the persistence activity of Northeast cold vortex in China. *Chin. J. Atmos. Sci.* **1997**, *21*, 297–307. (In Chinese)
4. Wang, D.H.; Zhong, S.X.; Liu, Y.; Li, J.; Hu, K.X.; Yang, S. Advances in the study of rainstorm in Northeast China. *Adv. Earth Sci.* **2007**, *22*, 549–560. (In Chinese)
5. Hu, K.X.; Lu, R.Y.; Wang, D.H. Seasonal climatology of cut-off lows and associated precipitation patterns over Northeast China. *Meteor. Atmos. Phys.* **2010**, *106*, 37–48. (In Chinese) [CrossRef]
6. Zhang, Q.; Tao, S.; Zhang, S. A study of excessively heavy rainfall in the Songhuajiang–Nenjiang River valley in 1998. *Chin. J. Atmos. Sci.* **2001**, *25*, 567–576. (In Chinese)
7. Sun, L.; An, G.; Gao, C.; Tang, X.L.; Ding, L.; Shen, B.Z. A composite diagnostic study of heavy rain caused by the Northeast cold vortex over Songhuajiang–Nenjiang River basin in summer of 1998. *Q. J. Appl. Meteorol.* **2002**, *13*, 156–162. (In Chinese)
8. Zhao, S.X.; Sun, J.H. Study on cut-off low-pressure systems with floods over Northeast Asia. *Meteor. Atmos. Phys.* **2007**, *96*, 159–180. [CrossRef]
9. Hu, K.; Lu, R.; Wang, D. Cold vortex over Northeast China and its climate effect. *Chin. J. Atmos. Sci.* **2011**, *35*, 179–191.

10. Ding, Y.H.; Li, J.S.; Sun, S.Q.; Cai, Z.Y.; Zhao, S.X.; Tao, S.Y. *The Analysis on Mesoscale Systems Producing Heavy Rainfall in North China*; Papers of Institute of Atmospheric Physics, Chinese Academy of Sciences, No. 9; Science Press: Beijing, China, 1980; pp. 1–13. (In Chinese)
11. Sun, J.; Zhang, X.; Wei, J.; Zhao, S.X. A study on severe heavy rainfall in North China during the 1990s. *Clim. Environ. Res.* **2005**, *10*, 492–506. (In Chinese)
12. Cong, C.; Chen, L.; Lei, X.; Li, Y. An overview on the study of tropical cyclone remote rainfall. *J. Trop. Meteorol.* **2011**, *27*, 264–270. (In Chinese)
13. Yan, M.; Zhao, K.; Jiao, L. The analysis on the Northeast cold vortex producing summer heavy rainfall in Heilongjiang Province. *Heilongjiang Meteorol.* **2005**, *3*, 30–31. (In Chinese)
14. Liang, Z.; Wang, D. A diagnostic study of a typhoon transitioning and merging into the Northeast cold vortex. *Chin. J. Atmos. Sci.* **2015**, *39*, 397–412. (In Chinese)
15. Zhou, G.; Liu, L.; Dong, L.; Wang, Q.; Xu, Y. The Analysis of Characteristics and Forecast Difficulties of TCs in Western North Pacific in 2020. *Meteorol. Monthly.* **2022**, *48*, 504–515. [CrossRef]
16. Du, H.; Ping, F.; Tan, G.; Zhou, G.; Huang, W.; Shen, X. Analysis of Microphysical Mechanisms of Torrential Rainfall during the Transitional Process of Typhoon Maysak (2020). *Chin. J. Atmos. Sci.* **2023**, *48*, 1–21. (In Chinese) [CrossRef]
17. Ren, L. Structural evolution characteristics and cause analysis of heavy rain of transition typhoon "Maysak". *Torrential Rain Disasters* **2023**, *42*, 521–531. (In Chinese) [CrossRef]
18. Fu, S.-M.; Sun, J.-H.; Qi, L.-L. Study on the Evolution of a Northeast China Cold Vortex during the Spring of 2010. *Atmos. Ocean. Sci. Lett.* **2014**, *7*, 149–156.
19. Li, W.; Shen, X.-Y.; Fu, S.-M.; Li, W.-L. Quadrant-Averaged Structure and Evolution Mechanisms of a Northeast Cold Vortex during Its Mature Stage. *Atmos. Ocean. Sci. Lett.* **2015**, *8*, 45–51.
20. Xu, H.; Xu, X.; Chen, B.; Chen, L.; Zhu, F. The structure change and energy moisture transport physical image in the development and decay processes of binary typhoon vortices. *Acta Meteorol. Sin.* **2013**, *71*, 825–838.
21. Yan, Q.; Cui, J.; Tan, Z.; He, B.-J. On the Contributions of the Northeast Cold Vortex to the Formation and Evolution of Backflow Blizzard. *Front. Earth Sci.* **2022**, *10*, 921043. [CrossRef]
22. Cheng, Z.Q.; Chen, L.S.; Li, Y. Diagnostic analysis of large-scale circulation features associated with strong and weak landfalling typhoon precipitation events. *Acta Meteorol. Sin.* **2009**, *67*, 840–850. (In Chinese) [CrossRef]
23. Li, Q.Q.; Wang, Y.Q. Formation and quasi-periodic behavior of outer spiral rainbands in a numerically simulated tropical cyclone. *J. Atmos. Sci.* **2012**, *69*, 997–1020. [CrossRef]
24. Liang, J.; Li, Y.; Zhang, S.J.; Liu, X.C. Comparison of synoptic circulations of heavy rain associated with typhoons Meari and Muifa over Liaodong Peninsula. *Chin. J. Atmos Sci.* **2015**, *39*, 1215–1224. (In Chinese)
25. Meng, W.G.; Wang, Y.Q. A diagnostic study on heavy rainfall induced by typhoon Utor (2013) in South China: 1. Rainfall asymmetry at landfall. *J. Geophys. Res.* **2016**, *121*, 12781–12802. [CrossRef]
26. Meng, W.G.; Wang, Y.Q. A diagnostic study on heavy rainfall induced by landfalling typhoon Utor (2013) in South China: 2. Postlandfall rainfall. *J. Geophys. Res.* **2016**, *121*, 12803–12819. [CrossRef]
27. Thompson, G.; Field, P.R.; Rasmussen, R.M.; Hall, W.D. Explicit forecasts of winter precipitation using an improved bulk microphysics scheme. Part II: Implementation of a new snow parameterization. *Mon. Weather Rev.* **2008**, *136*, 5095–5115. [CrossRef]
28. Dudhia, J. Numerical study of convection observed during the winter monsoon experiment using a mesoscale two-dimensional model. *J. Atmos. Sci.* **1989**, *46*, 3077–3107. [CrossRef]
29. Mlawer, E.J.; Taubman, S.J.; Brown, P.D.; Iacono, M.J.; Clough, S.A. Radiative transfer for inhomogeneous atmospheres: RRTM, a validated correlated-k model for the longwave. *J. Geophys. Res. Atmos.* **1997**, *102*, 16663–16682. [CrossRef]
30. Niu, G.Y.; Yang, Z.L.; Mitchell, K.E.; Chen, F.; Ek, M.B.; Barlage, M.; Kumar, A.; Manning, K.; Niyogi, D.; Rosero, E. The community Noah land surface model with multiparameterization options (Noah–MP): 1. Model description and evaluation with local–scale measurements. *J. Geophys. Res. Atmos.* **2011**, *116*, D12109. [CrossRef]
31. Hong, S.Y.; Noh, Y.; Dudhia, J. A new vertical diffusion package with an explicit treatment of entrainment processes. *Mon. Weather Rev.* **2006**, *134*, 2318–2341. [CrossRef]
32. Wang, C.; Gao, S.; Liang, Z.; Liang, L. Study and application of moist thermodynamic advection parameter to numerical simulation and diagnostic analysis of a rainstorm in North China. *Clim. Environ. Res.* **2014**, *19*, 753–762. (In Chinese)